A Feasibility Study of Single-inhalation, Single-energy Xenon-enhanced CT for High-resolution Imaging of Regional Lung Ventilation in Humans

Daniel W. Pinkham PhD[a] , Mohammadreza Negahdar PhD[ab], Tokihiro Yamamoto PhD[c], Erik Mittra MD, PhD[d], Maximilian Diehn MD, PhD[a], Viswam S. Nair MD, MS[e], Paul J. Keall PhD[f], Peter G. Maxim PhD[a], Billy W. Loo Jr.MD, PhD[a]

[a] Department of Radiation Oncology, Stanford University, 875 Blake Wilbur Dr., Stanford, CA 94305

[b]Almaden Research Center, IBM Research, San Jose, California

[c]Department of Radiation Oncology, University of California, Davis, Sacramento, California

[d]Department of Radiology, Stanford University, Stanford, California

[e]Division of Pulmonary & Critical Care Medicine, Stanford University, Stanford, California

[f]Radiation Physics Laboratory, The University of Sydney, NSW, Australia

Key Words

Computed tomography (CT), xenon, regional lung ventilation, single-photon emission computed tomography (SPECT)

Dr. Pinkham, Dr. Negahdar, and Dr. Yamamoto are equal contributors.

Funding: This study has been partly supported by National Institutes of Health (grant no. RO1 CA 093626) (PI: P. Keall) and by the Stanford University 2015 Bio-X Interdisciplinary Initiatives Seed Grant Program (PI: P. Maxim).

Rationale and Objectives

The objective of this study was to assess the feasibility of single-inhalation xenon-enhanced computed tomography (XeCT) to provide clinically practical, high-resolution pulmonary ventilation imaging to clinics with access to only a single-energy computed tomography scanner, and to reduce the subject's overall exposure to xenon by utilizing a higher (70%) concentration for a much shorter time than has been employed in prior studies.

Materials and Methods

We conducted an institutional review board-approved prospective feasibility study of XeCT for 15 patients undergoing thoracic radiotherapy. For XeCT, we acquired two breath-hold single-energy computed tomography images of the entire lung with a single inhalation each of 100% oxygen and a mixture of 70% xenon and 30% oxygen, respectively. A video biofeedback system for coached patient breathing was used to achieve reproducible breath holds. We assessed the technical success of XeCT acquisition and side effects. We then used deformable image registration to align the breath-hold images with each other to accurately subtract them, producing a map of lung xenon distribution. Additionally, we acquired ventilation single-photon emission computed tomography-computed tomography (V-SPECT-CT) images for 11 of the 15 patients. For a comparative analysis, we partitioned each lung into 12 sectors, calculated the xenon concentration from the Hounsfield unit enhancement in each sector, and then correlated this with the corresponding V-SPECT-CT counts.

Results

XeCT scans were tolerated well overall, with a mild (grade 1) dizziness as the only side effect in 5 of the 15 patients. Technical failures in five patients occurred because of inaccurate breathing synchronization with xenon gas delivery, leaving seven patients analyzable for XeCT and single-photon emission computed tomography correlation. Sector-wise correlations were strong (Spearman coefficient >0.75, Pearson coefficient >0.65, P value <.002) for two patients for whom ventilation deficits were visibly pronounced in both scans. Correlations were nonsignificant for the remaining five who had more homogeneous XeCT ventilation maps, as well as strong V-SPECT-CT imaging artifacts attributable to airway deposition of the aerosolized imaging agent. Qualitatively, XeCT demonstrated higher resolution and no central airway deposition artifacts compared to V-SPECT-CT.

Conclusions

In this pilot study, single-breath XeCT ventilation imaging was generally feasible for patients undergoing thoracic radiotherapy, using an imaging protocol that is clinically practical and potentially widely available. In the future, the xenon delivery failures can be addressed by straightforward technical improvements to the patient biofeedback coaching system.

Introduction

Xenon (Xe) is a radio-opaque and inert gas; therefore, it may be a viable and safe gas-phase computed tomography (CT) contrast agent to quantify regional pulmonary ventilation in humans. In order for such a contrast agent to be adopted widely, several clinical traits must be met: safety, convenience for the patient, and ease of implementation. Numerous studies have already explored the technical advantages of xenon-enhanced computed tomography (XeCT), such as its ability to provide reasonably safe high-resolution ventilation images. Dual-energy XeCT has been reported in patient and phantom studies (1- 5) but most XeCT studies, to date, have used a multiple breath-hold technique in which patients inhale xenon for 1–2 minutes to reach equilibrium before image acquisition and xenon washout (1- 4, 6).

There have also been research efforts to compare XeCT against currently available three-dimensional ventilation imaging, that is, single-photon emission computed tomography (SPECT) (7). Substantial agreement has recently been observed between XeCT and krypton-81m (Kr-81m) ventilation SPECT images in an intermodality blind analysis of lung ventilation defects (8). With this result lending further credence to the use of gas-phase CT contrast agents for ventilation imaging, we aim to further expand upon its potential for future clinical implementation. By increasing the relative xenon concentration by a factor of two relative to prior studies, but reducing the xenon exposure to a single breath-hold duration (a factor of 5 or more reduction in exposure time compared to the studies noted earlier), a more rapid image acquisition may be possible with an overall reduction in patients' total exposure to xenon gas, a known anesthetic agent.

We therefore developed a single-inhalation, single-energy XeCT imaging method for clinical practicality, and we conducted a feasibility study in patients undergoing thoracic radiation therapy. A preliminary comparison was conducted between the XeCT ventilation images and a clinically available ventilation imaging technique with an inhaled radioactive aerosol (ventilation single-photon emission computed tomography-computed tomography [V-SPECT-CT]).

Materials and Methods

Patients

In an institutional review board-approved prospective clinical study of feasibility, XeCT was acquired for 15 patients and V-SPECT-CT scans were acquired for 11 of the 15 patients. Eligible patients were those scheduled to undergo thoracic radiation therapy, and XeCT was acquired in conjunction with radiation therapy treatment planning scans. To administer xenon for this indication, we obtained an investigator-sponsored investigational new drug approval from the Food and Drug Administration for pulmonary CT imaging with xenon (investigational new drug no. 115882). Written informed consent was obtained from all patients before the administration of xenon. We characterized patients with chronic obstructive pulmonary disease (COPD) according to the Global Initiative for Chronic Obstructive Lung Disease (GOLD) criteria, which grades severity of disease based on pulmonary function tests from a scale of I to IV (9). Children and pregnant women were excluded from the present study.

Assessment of Adverse Events

Patient clinical status was assessed by a board-certified physician in radiation oncology (BWL) during and after the XeCT imaging session to monitor for adverse events. Side effects were scored by the common terminology criteria for adverse events (CTCAE v. 4.03).1

Relation of Hounsfield Unit and Xenon Concentration at Different X-ray Energies

A sealed rubber bag filled with eight different xenon and room air mixtures (0%, 5.83%, 11.7%, 23.3%, 35%, 46.7%, 58.3%, and 70% xenon) was scanned with a Biograph mCT PET/CT scanner (Siemens Medical Solutions, Hoffman Estates, IL) with five different x-ray energy

beams (70, 80, 100, 120, and 140 kV) at room temperature. Images were acquired using a tube current of 200 mAs, with 1.2-mm slice thickness, and medium smooth reconstruction kernel (B30s).

Video Biofeedback System

A custom video biofeedback system was used to facilitate achieving reproducible deep inhalation breath-hold levels to minimize errors in image alignment (10). Before the administration of the xenon gas and scans, patients were given instructions by the study investigators, familiarized with the ventilation apparatus, and allowed to practice breath holds with oxygen without administering xenon gas.

XeCT Imaging

Breath-hold CT scans were acquired on a Biograph mCT PET/CT scanner (Siemens Medical Solutions), using the following settings: 80 kVp (100 kVp for two patients), 125–325 mAs (195 mAs for eight patients), 2-mm slice thickness, 0.97×0.97 mm^2 pixel size, and a smooth reconstruction kernel (B20f).

Xe-O_2 was delivered to the patient using a gas delivery system as shown in Figure 1. The mouthpiece assembly was designed to have a minimum amount of dead space, thereby allowing a more efficient delivery of contrast agent to the patient's lungs. The inhalation gas was switched between Xe-O_2 and O_2 by opening and closing balloon valves that were remotely controlled at the on-site workstation. An infrared reflector (RPM; Varian Medical Systems, Palo Alto, CA) was placed on each patient's abdomen to provide a breathing trace to cue the investigators to toggle between the ventilation gases. XeCT imaging protocols consisted of (1) acquisition of a breath-hold CT scan after a single inhalation of 100% oxygen and (2) acquisition of a breath-hold CT scan after a single inhalation of a 70% xenon-30% oxygen mix. Patients were coached to exhale completely before each inhalation breath hold.

Deformable Image Registration Method

To minimize interscan variability when performing image subtraction between pre– and post–xenon inhalation scans, we developed an intensity-based free-form deformable image registration (DIR) workflow using the Elastix toolkit (11, 12). We coregistered the breath-hold images before and after inspiration of xenon (13, 14), and we employed lung masks and a multiscale vesselness filter (15) to further guide the intensity-based deformation process. Lung masks were generated using a Hounsfield unit window between −1024 and −300 HU. The lung vasculature was included in the DIR masks via morphologic closing of the Hounsfield unit-defined contours, but was subsequently excluded from statistical analyses where regional ventilation of the parenchyma was being assessed. Visual inspection was performed on the deformation vector field to verify the absence of nonphysical transformations (such as folding or tearing). Figure 2a and b illustrates how the two sequential CT images are combined to form difference images without (Fig 2c) and with (Fig 2d) DIR.

SPECT-CT Imaging

V-SPECT-CT was performed by the standard clinical protocol at our institution. Forty millicurie of 99m Tc-DTPA was aerosolized using a standard technique, and approximately 1 mCi was inhaled by the patient in a supine position with slow, moderately deep breathing. SPECT-CT images were then acquired using a GE Infinia Hawkeye 8-slice SPECT-CT scanner (Milkwaukee, WI). SPECT projections were acquired in a 64×64 matrix with an $8.84 \times 8.84\ mm^2$ pixel size, 8.84-mm slice spacing, 60 projections over 360°, and 30 seconds per projection during tidal breathing, for a total of 300K counts. The SPECT images were reconstructed with attenuation correction using the CT images.

Analysis of XeCT Images and Correlation with V-SPECT-CT

After image acquisition, DIR spatially aligned the two breath-hold images with each other. Then Xe concentration was calculated by subtraction between Xe-O_2 and O_2 images, which yields a high-resolution map of regional distribution of Xe. Each of the XeCT quantitative images of regional lung ventilation and their physiological accuracy was compared to aerosol-based V-SPECT-CT, a technique for the generation of ventilation imagery that is widely available but has known limitations (16).

As shown in Figure 3, each lung was divided into 12 sectors and correlated with the mean Hounsfield unit enhancement at each sector with the median V-SPECT-CT count of the corresponding sector of the lung. The Spearman rank correlation coefficient, a nonparametric measure of statistical dependence, and the Pearson linear correlation coefficient, a measure of the strength of linear dependence, were determined to quantify the correlation between each pair of scans.

Statistical Analysis

The data, consisting of XeCT and V-SPECT-CT, were analyzed in a hierarchical model with repeated measurements within patients and with the assumption that the variance-covariance structure followed a compound symmetry structure. The Spearman rank correlation coefficient and the Pearson linear correlation coefficient were determined to quantify the correlation between XeCT and V-SPECT-CT images. All analyses were performed using the Scipy statistics package for Python (version 3.5).

Results

Patient Characteristics

Between December 2013 and July 2014, 15 patients (11 men and 4 women) met the eligibility criteria and were enrolled in the study. Patient characteristics are summarized in Table 1. Their age ranged from 55 to 79 (66 ± 7) years. One patient had no pulmonary function test and nine patients had COPD, across all GOLD stages with a forced expiratory volume of 39–107 (65 ± 20). The cohort average lung volume was 5.3 ± 1.6 L. Eleven of the 15 patients consented to acquisition of both XeCT and V-SPECT-CT scans (designated as patients 1–11). Four patients had XeCT only (designated as patients X1–X4).

Technical Feasibility and Side Effects

We successfully obtained XeCT images for 10 of the 15 patients. Patients 2, 4, 10, 11, and X4 had technical failure of XeCT because of inaccurate synchronization of inhalation with Xe gas delivery: in one case, the patient inhaled room air around the mouthpiece of the gas delivery system at the time of xenon delivery. Subsequently, we switched to the use of snorkel mouthpieces to prevent open-mouth breathing. The remaining four patients with technical failures had incorrect determination of completeness of exhalation before xenon inhalation with the existing biofeedback system, leading to an incorrect timing of xenon inhalation. Because of the higher experimental concentration of xenon, the patients were not asked to repeat the inhalation-scanning procedure, and these cases were subsequently logged as technical failures. Successful inhalation of the xenon mixture was confirmed by measurement of the xenon concentration in the central airways (shown with the lung masks in Fig A1 and tabulated in Table 1). Five of 15 patients experienced transient grade 1 dizziness lasting less than 1 minute immediately after the breath hold of the Xe gas mixture that resolved after switching back to oxygen breathing. There were no other side effects.

Relation of Hounsfield Unit and Xenon Concentration at Different X-ray Energies

The mean Hounsfield units of voxels within the inflatable rubber bag were measured in each image set at each xenon concentration and were plotted against the xenon concentration for different x-ray energies. The mean Hounsfield units of the xenon in the bag were linearly related to xenon concentration as apparent in Figure 4. Slopes and intercepts of linear regression equations and regression coefficients (R^2) were, respectively, 2.46, −1000.4, and 0.99 for 70-kV images; 2.16, −1001, and 0.99 for 80-kV images; 1.70, −1000, and 0.99 for 100-kV images; 1.43, −999.89, and 0.99 for 120-kV images; and 1.27, −1000.4, and 0.99 for 140-kV images. The maximum enhancement was 175 HU for a xenon concentration of 70% at 70 kV.

Ventilation Maps

Table 1 shows the Spearman correlation coefficients and the Pearson correlation coefficients between the mean xenon concentration and the V-SPECT-CT counts at corresponding sectors for each patient. The single-breath xenon inspiration was deemed to be successful when the mean Hounsfield unit difference within the trachea and the primary bronchial tree was greater than 80 HU. Patients who achieved a successful inspiration displayed a difference of 116 ± 16 HU, whereas patients with technical failures exhibited a difference of 16 ± 19 HU. Figure 5 shows the corresponding coronal XeCT and V-SPECT-CT images, along with the calculated correlation between XeCT and V-SPECT-CT at the corresponding sectors for two patients (patients 1 and 8) with images displaying a high degree of heterogeneity of ventilation throughout the lungs. There was a clear visual concordance (and strong Spearman correlation coefficient) between the two image modalities for these patients. Figure A1 in the Appendix shows the corresponding coronal XeCT and V-SPECT-CT image pairs for all patients in our study who underwent both types of scan (designated as patients 1–11), along with a plot of the ventilation signals from corresponding sectors of the two imaging studies. Notably, patients 3, 5, 6, 7, and 9 demonstrated much more homogeneous XeCT ventilation maps than patients 1 and 8. Figure A2 in the Appendix shows the corresponding coronal XeCT for patients who had XeCT only (designated patients X1-X4).

Discussion

We have developed an imaging method to determine the spatial distribution of xenon gas (during a single 70% xenon inhalation maneuver) as a measure of regional ventilation, and conducted here a first in human feasibility study of the method in a single-energy CT scanner. Single-inhalation, single-energy XeCT was technically successful in 10 of 15 patients, and the five technical failures were attributable to incorrect synchronization between the inhalation and the delivery of the Xe gas mixture. These failures can be corrected in the future by improvements to the biofeedback system, such as increased patient training, as well as the implementation of a spirometry-based breathing surrogate signal that measures the volume of air moved as a surrogate for the degree of lung expansion. This approach would provide a more ideal feedback signal than our currently implemented infrared reflector positioned on the patient's abdomen.

Finally, we compared XeCT ventilation to V-SPECT-CT, which is a clinically available three-dimensional ventilation imaging modality. The voxel values of the xenon-enhanced images were related to the degree of ventilation magnitude. Of seven evaluable patients, two (patients 1 and 8) had a high correlation between regional Xe concentration and SPECT emission counts. For patient 8, paralysis of the left hemidiaphragm was associated with decreased ventilation throughout the entire left lung. In contrast, five patients (patients 3, 5, 6, 7, and 9) demonstrated low correlation between XeCT and V-SPECT-CT. These patients had either normal (patients 3 and 5) or diminished (patients 6, 7, and 9) lung function as assessed by spirometry, but with homogeneous distribution. Because ventilation between sectors was relatively homogeneous, any observed variability is dominated by random noise; therefore, when these XeCT images are compared on a sector-wise basis with alternate image modalities, strong Spearman correlations are unlikely to be observed. The different parameters for contrast administration (deep-inspiration breath hold of a gaseous agent vs free breathing of a nebulized aerosol) suggest that perfect correlation may not actually be achievable when comparing the two imaging modalities. Furthermore, the relatively narrow spread of xenon ventilation signal (the y-axis ranges observed in the Fig A1 subplots) is small compared to the dynamic range of the SPECT counts (x-axis ranges). This finding would make the intermodality correlation more susceptible to the bright central airway artifacts that are seen in the corresponding SPECT images.

Our proposed single breath-hold single-energy CT method for quantifying regional lung ventilation demonstrates several benefits. With only a single xenon inhalation, we can use a higher concentration of xenon (70% xenon and 30% oxygen) than possible with previous XeCT techniques and observe no side effects other than transient (Grade 1) dizziness while simultaneously providing greater contrast and dynamic range compared to prior studies 5, 17 and better sensitivity at low ventilation regions. We chose 80 kVp to trade between higher attenuation by xenon (Fig 4) and better quality anatomic imaging of the lung. The use of a single-energy CT scanner also makes this method widely accessible.

Furthermore, with the use of video biofeedback for improved breath-hold reproducibility, only a minimal application of lung deformable registration is needed, and this is easily achieved by most commercial DIR software packages. For example, the image processing workflow and analysis from the present study was fully replicated (except for the vesselness-based registration mask) using a commercially available MIM Maestro package (MIM Software Inc., Cleveland,

OH) that has been optimized for clinical use. Similar results were obtained, with patients 1 and 8 again demonstrating the strongest sector-wise Spearman correlations with V-SPECT-CT ($\rho \geq 0.75$, $P < .001$), although these XeCT ventilation images (generated with clinical software) have more pronounced blood vessel misregistration artifacts throughout the lungs. The coarse scaling of the sector-wise analysis (12 segments per lung) is apparently robust to minor registration artifacts that impact only a small fraction of each lung sector.

Despite many recent advances in medical imaging technology, there is no clinical imaging method that permits quantitative high-resolution regional assessment of ventilation within the lung. Hence, a broadly available high-resolution quantitative functional imaging method is needed. For patients suffering from lung cancer treated with radiation therapy, regional ventilation may be used for tracking the progression of radiation-induced toxicity to nearby normal tissues during treatment and can be used to evaluate treatment planning methods to reduce radiation toxicity to the most functional portions of the lung (18- 23). Regional lung function information may also be used for lung disease therapy planning, such as lung volume reduction surgery, to improve lung biomechanics and the quality of life for certain patients with emphysema or to optimize ventilator management for patients with acute respiratory distress syndrome (24). Regional lung function information may also be useful for the diagnosis and monitoring of pulmonary diseases such as COPD (25).

Nuclear medicine imaging (most commonly planar imaging) is a commonly utilized technique for ventilation assessment. By comparison, advantages of the XeCT method demonstrated in the present study include higher resolution, volumetric imaging, improved quantitation, shorter study time, and lack of aerosol deposition artifacts in the airways. Notably, newer radiolabeled gases or aerosols for use with nuclear medicine ventilation imaging such as Ga-68 aerosol (Galligas) (26, 27), an ultrafine dispersion of 99m Tc-labeled carbon (Technegas) (28, 29), and radioactive Xe-133 gas (30) can reduce airway deposition artifacts, but are not currently approved for clinical use in the United States.

Different gases have been used as gas-phase contrast agents for pulmonary imaging, including krypton (31, 32) and xenon (1-5, 29). However, these methods have typically used either dual-energy CT scanners or hyperpolarized MRI, which require specialized equipment that is not widely available, or used longer wash-in times for contrast inhalation. The recent work by Ohno et al. with a gas-phase (krypton) SPECT contrast agent is an encouraging affirmation of the equivalence between XeCT and SPECT, and their mode of contrast agent delivery is also not impacted by aerosol deposition artifacts (8). A significant proportion of the patient population undergoing thoracic radiotherapy presents with obstructive disease that can trap aerosols in the central airways, so it is likely that gaseous contrast agents will find better application within the radiation oncology field.

The size of our patient cohort is the primary limitation of the present study. Larger studies will be required for comprehensive validation. Furthermore, the dose of a XeCT scan at 80 kVp with sufficient exposure to match the noise characteristics of a standard diagnostic chest CT is

approximately 4.2 mSv, which is significantly higher than that of V-SPECT-CT at 0.7 mSv. Nevertheless, the dose is still lower than a standard diagnostic chest CT acquired at 120 kVp (approximately 9.3 mSv).

In conclusion, single-inhalation, single-energy XeCT has the potential to quantify regional lung ventilation volumetrically and with high resolution using widely accessible radiological equipment. Higher concentrations of inhaled xenon (70%) can be safely administered and can provide enough contrast such that only a single inspiration may be necessary to characterize regional lung defects. Clinically available medical image analysis software can be utilized to process XeCT ventilation images.

References

1. Chae EJ, Seo JB, Goo HW, et al. Xenon ventilation CT with a dual energy technique of dual-source CT: initial experience. Radiology 2008; 248:615–624.

2. Park E-A, Goo JM, Park SJ, et al. Chronic obstructive pulmonary disease: quantitative and visual ventilation pattern analysis at xenon ventilation CT performed by using a dual-energy technique. Radiology 2010; 256:985– 997.

3. Goo H, Yang D, Hong S-J, et al. Xenon ventilation CT using dualsource and dual-energy technique in children with bronchiolitis obliterans: correlation of xenon and CT density values with pulmonary function test results. Pediatr Radiol 2010; 40:1490–1497.

4. Thieme S, Hoegl S, Nikolaou K, et al. Pulmonary ventilation and perfusion imaging with dual-energy CT. Eur Radiol 2010; 20:2882–2889.

5. Honda N, Osada H, Watanabe W, et al. Imaging of ventilation with dualenergy CT during breath hold after single vital-capacity inspiration of stable xenon. Radiology 2012; 262:262–268.
6. Murphy DM, Nicewicz JT, Zabbatino SM, et al. Local pulmonary ventilation using nonradioactive xenon-enhanced ultrafast computed tomography. Chest 1989; 96:799–804.

7. Yanagita H, Honda N, Nakayama M, et al. Prediction of postoperative pulmonary function: preliminary comparison of single-breath dualenergy xenon CT with three conventional methods. Jpn J Radiol 2013; 31:377–385.

8. Ohno Y, Yoshikawa T, Takenaka D, et al. Xenon-enhanced CT using subtraction CT: basic and preliminary clinical studies for comparison of its efficacy with that of dual-energy CT and ventilation SPECT/CT to assess regional ventilation and pulmonary functional loss in smokers. Eur J Radiol 2017; 86:41–51.

9. Gomez FP, Rodriguez-Roisin R. Global Initiative for Chronic Obstructive Lung Disease (GOLD) guidelines for chronic obstructive pulmonary disease. Curr Opin Pulm Med 2002; 8:81–86.

10. Yu AS, von Eyben R, Yamamoto T, et al. Anatomic optimization of lung tumor stereotactic ablative radiation therapy. Pract Radiat Oncol 2015; 5:e607–e613.

11. Klein S, Staring M, Murphy K, et al. Elastix: a toolbox for intensitybased medical image registration. IEEE Trans Med Imaging 2010; 29:196– 205.

12. Shamonin DP, Bron EE, Lelieveldt BP, et al. Disease neuroimaging, fast parallel image registration on CPU and GPU for diagnostic classification of Alzheimer's disease. Front Neuroinform 2013; 7:50.

13. Nie K, Chuang C, Kirby N, et al. Site-specific deformable imaging registration algorithm selection using patient-based simulated deformations. Med Phys 2013; 40:041911.

14. Negahdar M, Fasola CE, Yu AS, et al. Noninvasive pulmonary nodule elastometry by CT and deformable image registration. Radiother Oncol 2015; 115:35–40.

15. Sato Y, Nakajima S, Shiraga N, et al. Three-dimensional multi-scale line filter for segmentation and visualization of curvilinear structures in medical images. Med Image Anal 1998; 2:143–168.

16. Schembri GP, Roach PJ, Bailey DL, et al. Artifacts and anatomical variants affecting ventilation and perfusion lung imaging. Semin Nucl Med 2015; 45:373–391.

17. Sase S, Nakano H, Suzuki H, et al. Subtraction lung image for evaluating pulmonary ventilation in xenon-enhanced CT. Med Phys 2010; 37:4464–4474.

18. Ding K, Bayouth JE, Buatti JM, et al. 4DCT-based measurement of changes in pulmonary function following a course of radiation therapy. Med Phys 2010; 37:1261–1272.

19. Munawar I, Yaremko BP, Craig J, et al. Intensity modulated radiotherapy of non-small-cell lung cancer incorporating SPECT ventilation imaging. Med Phys 2010; 37:1863–1872.

20. Huang T-C, Hsiao C-Y, Chien C-R, et al. IMRT treatment plans and functional planning with functional lung imaging from 4D-CT for thoracic cancer patients. Radiat Oncol 2013; 8:3.

21. Bates EL, Bragg CM, Wild JM, et al. Functional image-based radiotherapy planning for non-small cell lung cancer: a simulation study. Radiother Oncol 2009; 93:32–36.

22. Vinogradskiy Y, Schubert L, Diot Q, et al. Regional lung function profiles of stage I and III lung cancer patients: an evaluation for functional avoidance radiation therapy. Int J Radiat Oncol 2016; 95:1273– 1280.

23. Yamamoto T, Kabus S, Bal M, et al. The first patient treatment of computed tomography ventilation functional image-guided radiotherapy for lung cancer. Radiother Oncol 2016; 118:227–231.

24. Bellani G, Rouby JJ, Constantin JM, et al. Looking closer at acute respiratory distress syndrome: the role of advanced imaging techniques. Curr Opin Crit Care 2017; 23:30–37.

25. Hwang HJ, Seo JB, Lee SM, et al. Assessment of regional xenon ventilation, perfusion, and ventilation-perfusion mismatch using dualenergy computed tomography in chronic obstructive pulmonary disease patients. Invest Radiol 2016; 51:306–315.

26. Hofman MS, Beauregard J-M, Barber TW, et al. 68Ga PET/CT ventilation–perfusion imaging for pulmonary embolism: a pilot study with comparison to conventional scintigraphy. J Nucl Med 2011; 52:1513– 1519.

27. Ament SJ, Maus S, Reber H, et al. PET lung ventilation/perfusion imaging using (68)Ga aerosol (Galligas) and (68)Ga-labeled macroaggregated albumin. Recent Results Cancer Res 2013; 194:395– 423.

28. Bajc M, Neilly JB, Miniati M, et al. EANM guidelines for ventilation/perfusion scintigraphy: part 1. Pulmonary imaging with ventilation/perfusion singlephoton emission tomography. Eur J Nucl Med Mol Imaging 2009; 36:1356– 1370.

29. Jogi J, Jonson B, Ekberg M, et al. Ventilation-perfusion SPECT with 99mTcDTPA versus Technegas: a head-to-head study in obstructive and nonobstructive disease. J Nucl Med 2010; 51:735–741.

30. Parameswaran K, Knight AC, Keaney NP, et al. Ventilation and perfusion lung scintigraphy of allergen-induced airway responses in atopic asthmatic subjects. Can Respir J 2007; 14:285–291.

31. Hachulla A-L, Pontana F, Wemeau-Stervinou L, et al. Krypton ventilation imaging using dual-energy CT in chronic obstructive pulmonary disease patients: initial experience. Radiology 2012; 263:253–259.

32. Chon D, Beck KC, Simon BA, et al. Effect of low-xenon and krypton supplementation on signal/noise of regional CT-based ventilation measurements. J Appl Physiol 2007; 102:1535–1544.

TABLE 1. Individual Patient Data

Patient	Gender	Xe~V-SPECT-CT Spearman Coefficient (*P* Value)	Xe~V-SPECT-CT Pearson Coefficient (*P* Value)	Mean Xenon Enhancement: Trachea (HU)	Lung Volume (L, at Inspiration)	Lung Volume Difference (%) (Xe vs O_2)	FEV_1%	COPD (GOLD Score)
1	M	0.79 (.000007)	0.72 (.00011)	97.8	7.9	−4.0	39	3
2*	M	−0.34	−0.16	10.3	5.1	−1.0	61	1
3	F	0.27 (.21)	0.51 (.013)	115.1	3.9	1.2	79	No COPD
4*	M	0.39	0.51	16.5	4.2	−25.8	60	1
5	M	0.02 (.92)	0.004 (.98)	131.0	7.1	11.8	107	No COPD
6	M	0.19 (.37)	0.15 (.48)	113.3	4.6	−1.4	59	No COPD
7	F	−0.3 (.18)	−0.16 (.47)	127.2	3.7	13.7	64	1
8	M	0.75 (.00009)	0.65 (.0014)	134.2	6.0	0.9	62	1
9	M	0.33 (.12)	0.4 (.059)	100.8	8.2	−4.1	59	2
10*	M	−0.04	0.02	47.0	5.1	3.1	No PFT	No PFT
11*	F	0.45	0.27	−2.4	3.2	−7.5	59	2
X1	M	—	—	118.5	6.2	−1.4	75	1
X2	M	—	—	87.0	3.6	10.5	81	No COPD
X3	F	—	—	132.2	6.1	−0.4	21	4
X4*	M	—	—	6.4	4.4	0.4	87	No COPD

COPD, chronic obstructive pulmonary disease; F, female; FEV_1%, forced expiratory volume; GOLD, Global Initiative for Chronic Obstructive Lung Disease; M, male; PFT, pulmonary function test; V-SPECT, ventilation single-photon emission computed tomography.

The third and fourth columns show the Spearman correlation coefficients (*P* value) and the Pearson correlation coefficients (*P* value), respectively, between xenon concentration and single-photon emission computed tomography ventilation image at corresponding sectors. The fifth and sixth columns show the Hounsfield unit enhancement in the trachea and the lung volumedifference from the consecutive computed tomography images. The eighth and ninth columns show the PFT FEV_1% and GOLD score for each patient, respectively. Patients X1–X4 participated in xenon-enhanced computed tomography imaging, but have no single-photon emission computed tomography ventilation. Patients 2, 4, 10, 11, and X4 had technical failure of xenon-enhanced computed tomography and were excluded from the correlation analysis. The patient ages ranged from 55 to 79 years (average 66 ± 7 years).

* Technical failures.

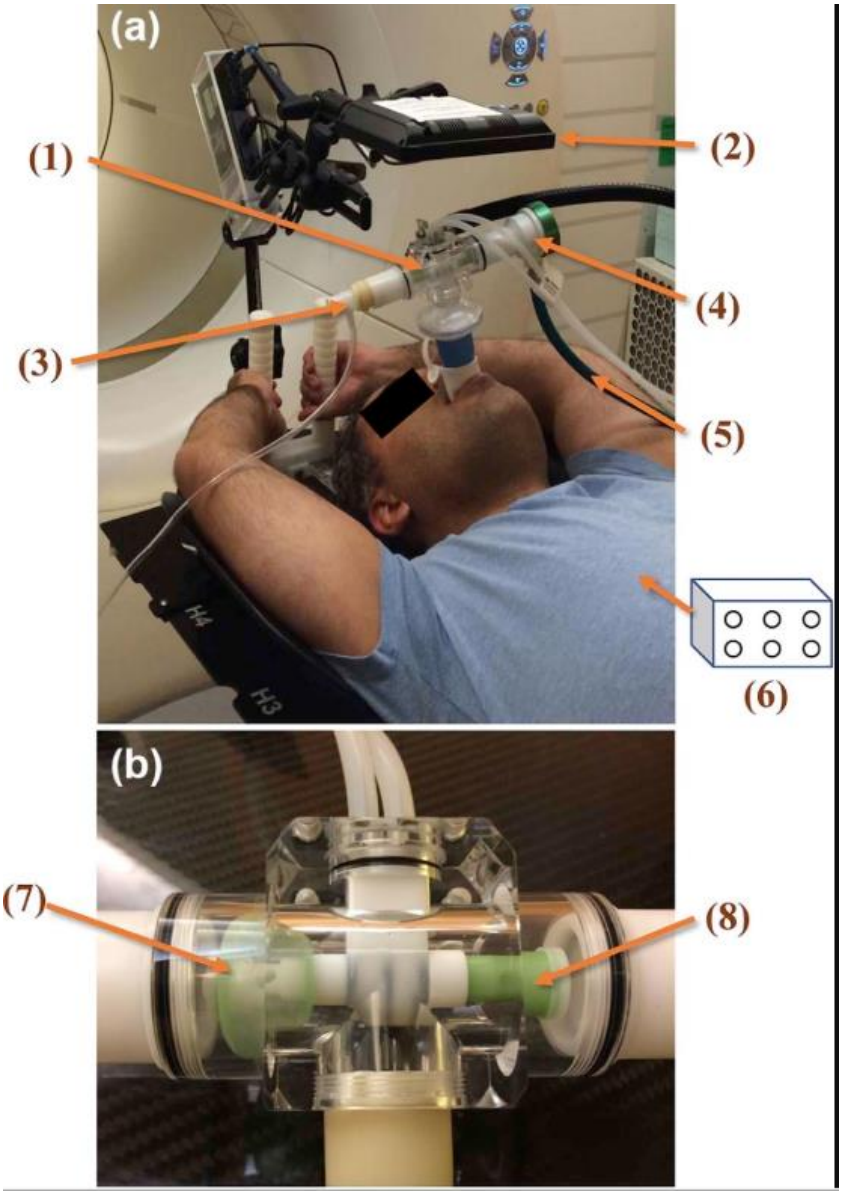

Figure 1. Experimental apparatus—picture of a Xe-O_2 delivery system (a) with one of the principal investigators demonstrating its use. The inhalation gas can be switched between Xe-O_2 and O_2 by opening and closing the balloon valves (b), which are controlled remotely by the balloon valve controller. The application of this ventilation apparatus was integrated into the clinical simulation workflow, and the hardware can all easily fit onto a small pushcart adjacent to the computed tomography couch. Although the apparatus is depicted with the patient's arms up, it could easily be modified for arms-down use for patients. Arrows in the figure point to (1) the balloon valve, (2) the video biofeedback apparatus, (3) the oxygen supply line, (4) the xenon demand valve, (5) the xenon-oxygen supply line, (6) the infrared reflector (not depicted), (7) an inflated, closed balloon valve, and (8) a deflated, open balloon valve.

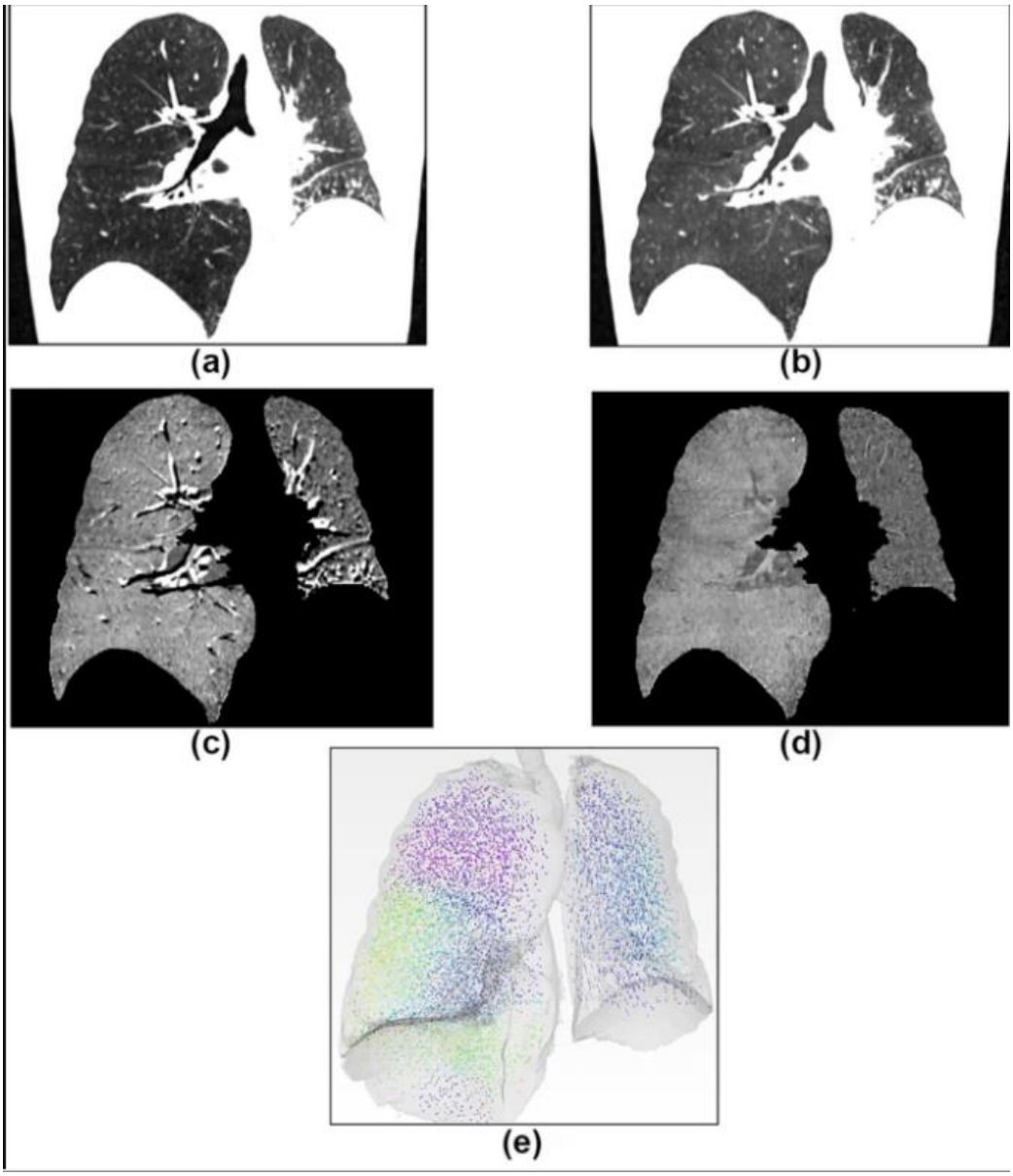

Figure 2. Ventilation images—two end-inspiratory breath-hold images acquired sequentially for patient 8 with a paralyzed left hemidiaphragm: (a) O_2 breath-hold image and (b) Xe breath-hold computed tomography image. The masked difference images are shown (c) before and (d) after applying deformable image registration. Vessel registration mismatch artifacts manifest as adjacent bright and dark lines, which are subsequently reduced with vessel-guided deformable image registration. Image (e) shows the three-dimensional displacement vector map between the two subsequent inspiration computed tomography scans with O_2 and Xe. Because of the inspiration reproducibility gained with the video biofeedback system, the required deformation was minimal between the two breath-hold scans.

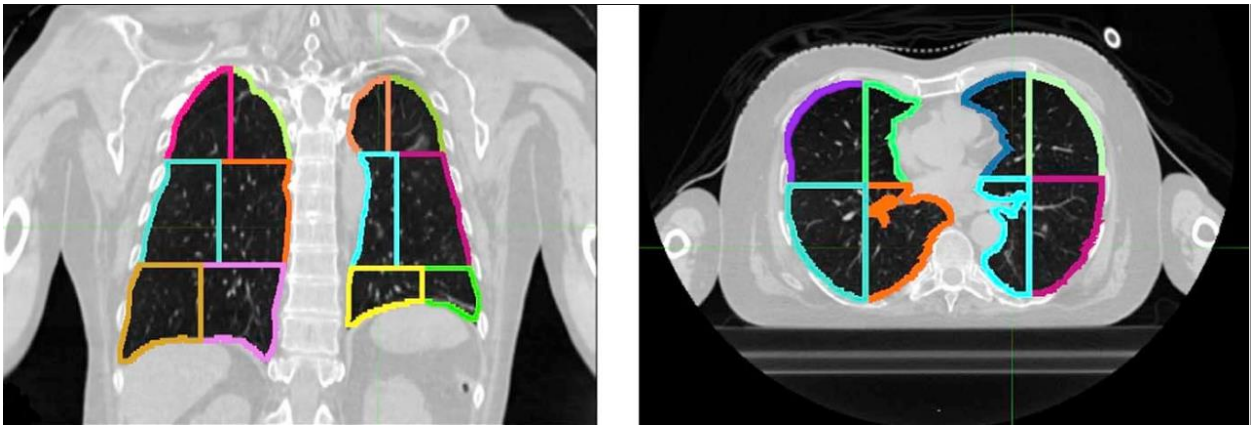

Figure 3. Lung partitioning: lungs were divided into 12 sectors each for analysis (superior, middle, and inferior, each divided into quadrants, for a total of 24 sectors per patient) on both xenon-enhanced computed tomography and ventilation single-photon emission computed tomography-computed tomography, and the mean values of xenon concentration and single-photon emission computed tomography emission counts of corresponding sectors were correlated. This partitioning was chosen specifically to be sensitive to larger ventilation deficits and to be more robust to any residual voxel-wise deformation artifacts. Left image, coronal planar view of the lung partitions. Right image, axial planar view of the lung partitions.

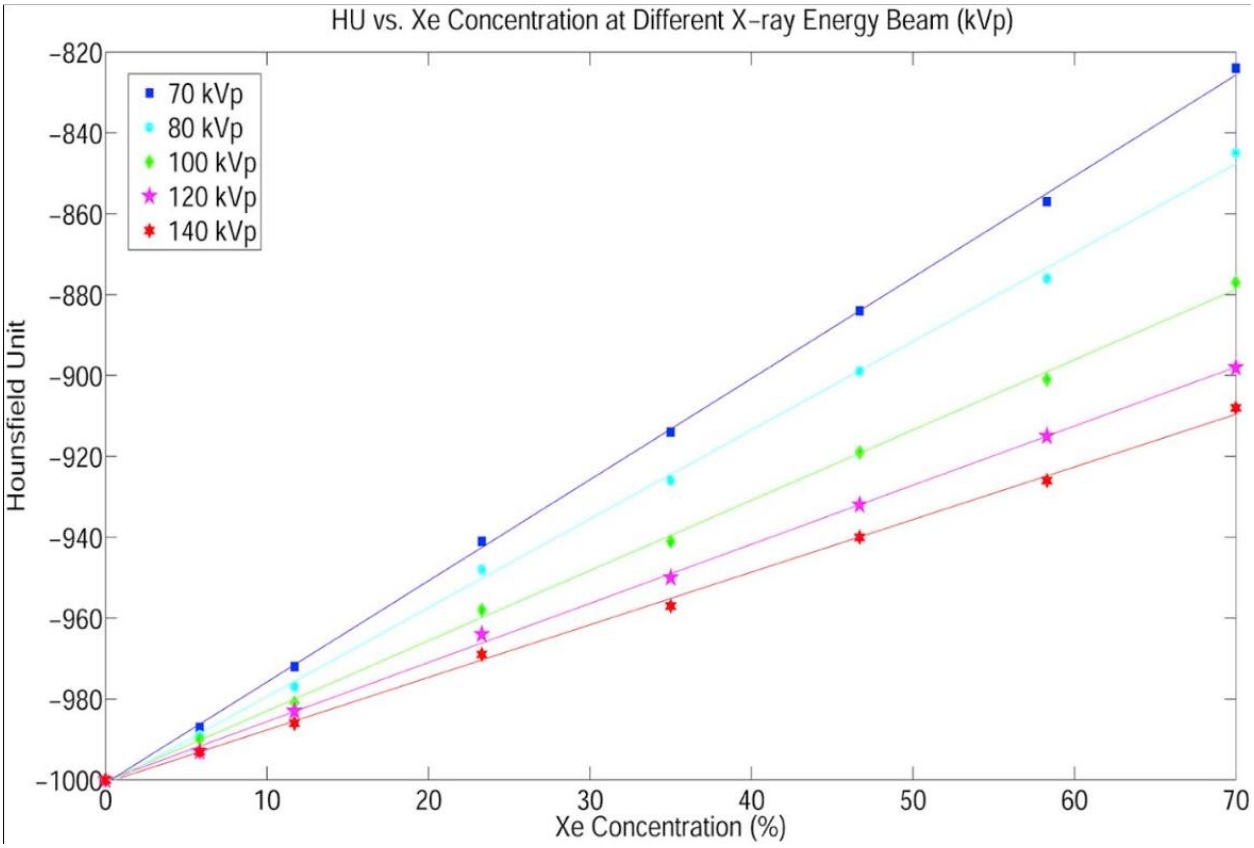

Figure 4. Xenon concentration measurement—relation of computed tomography numbers (Hounsfield units) to xenon concentration at different x-ray energies (kVp). The primary x-ray energy for the majority of patients in this study was chosen to be 80 kVp, which yields a maximum Hounsfield unit difference of about 150 HU. The plotted curves (from top to bottom) correspond to 70-, 80-, 100-, 120-, and 140-kVp tube voltages, respectively.

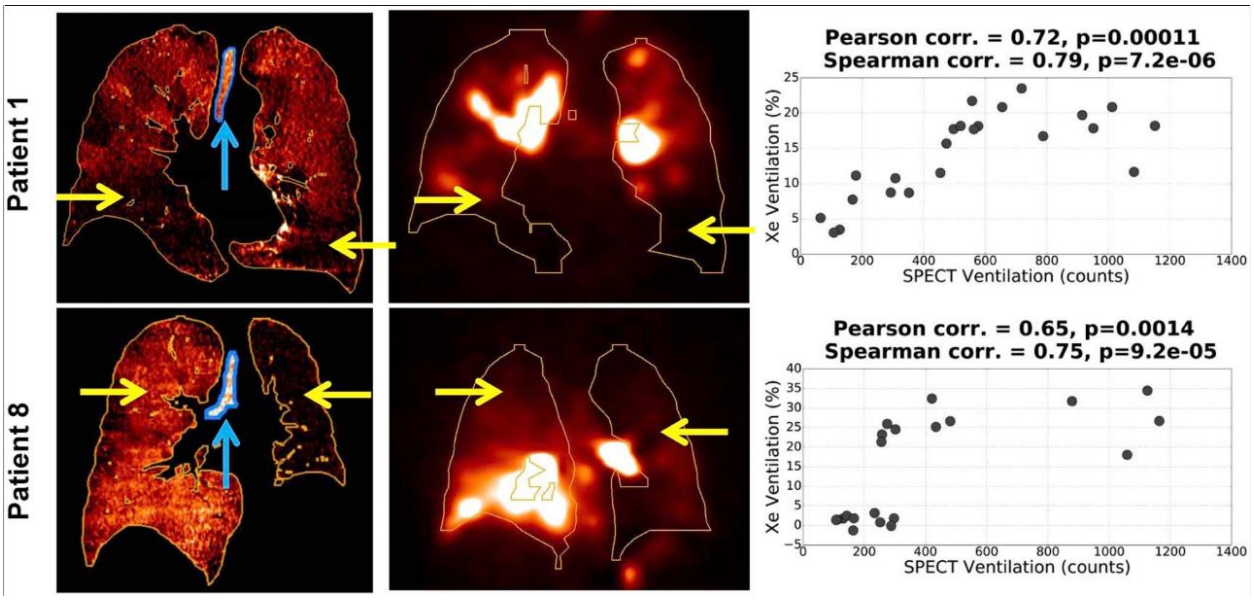

Figure 5. Corresponding coronal views of XeCT images along with V-SPECT for two patients who exhibited ventilation defects that were clearly visible in both imaging modalities. Left column, XeCT images: yellow arrows show areas of low xenon concentration within the lung due to ventilation deficits; blue arrows point to the highlighted Hounsfield unit enhancement visible in the trachea, which enabled the determination of successful uptake of the xenon contrast. Middle column, V-SPECT images: yellow arrows point out the ventilation deficits in V-SPECT. Right column, comparison plots: the plotted relationship between XeCT and V-SPECT for corresponding subsectors in the lung. This sector-wise comparison method is easily able to detect large-scale deficiencies in regional lung ventilation. SPECT, single-photon emission computed tomography; XeCT, xenon-enhanced computed tomography; V-SPECT, ventilation single-photon emission computed tomography.

Supplementary Information

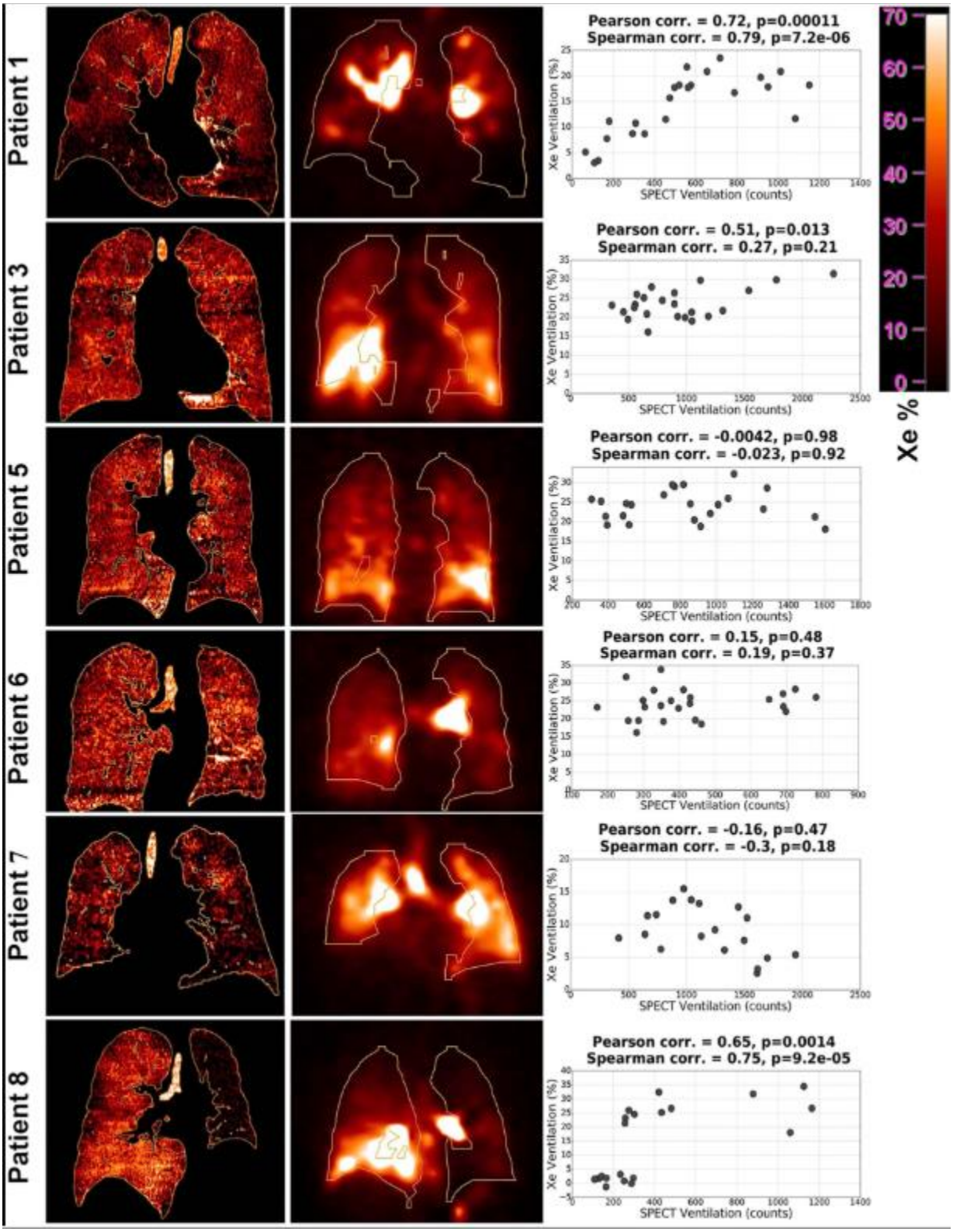

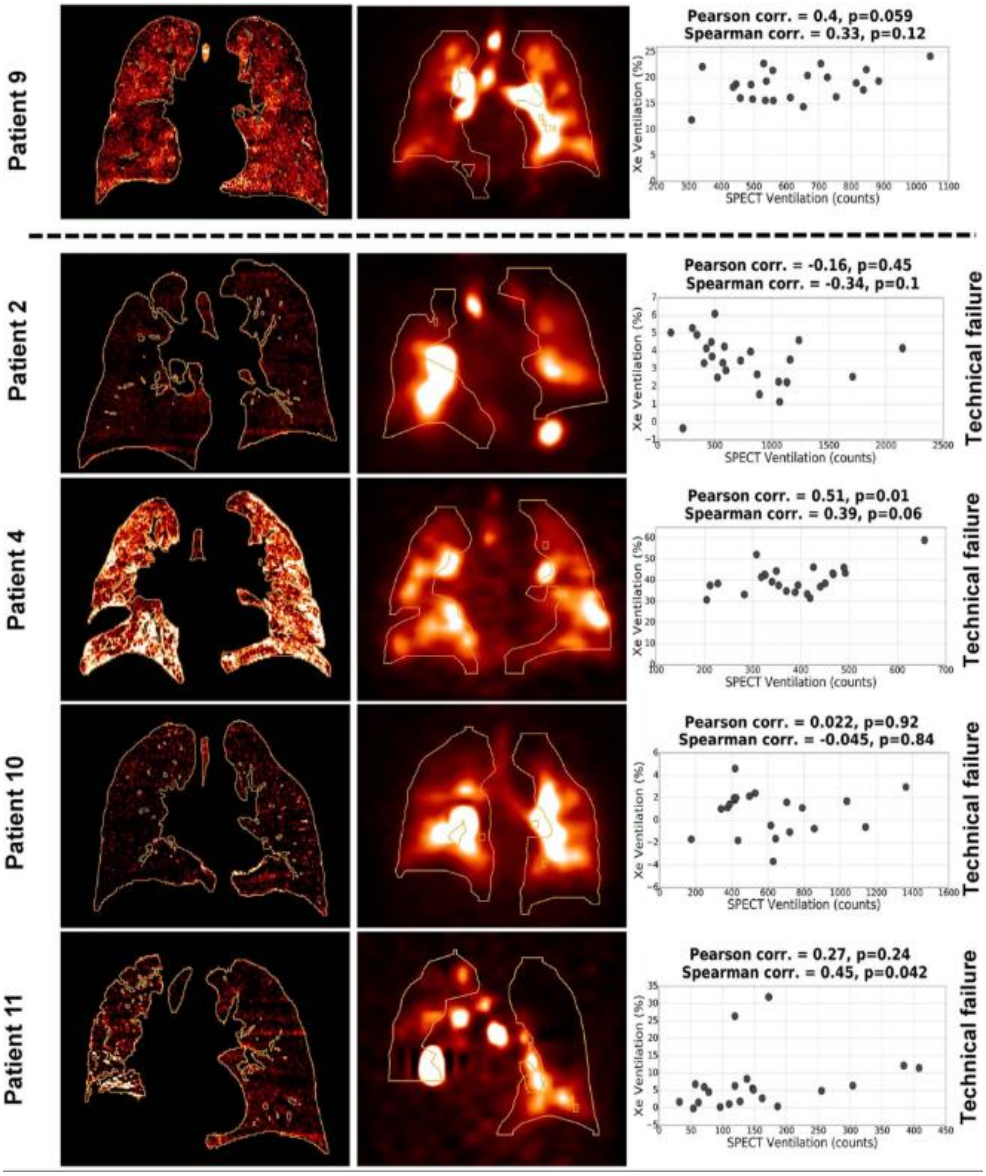

Figure A1. Patient imaging—xenon-enhanced computed tomography ventilation image (left column) along with SPECT ventilation image (the clinical standard) (middle column) and the correlation between xenon-enhanced computed tomography image with ventilation SPECT-computed tomography image at the corresponding sectors (right column) for all 11 patients who underwent both scans. Elevated trachea Hounsfield unit values are visible in the successful xenon scans. SPECT, single-photon emission computed tomography.

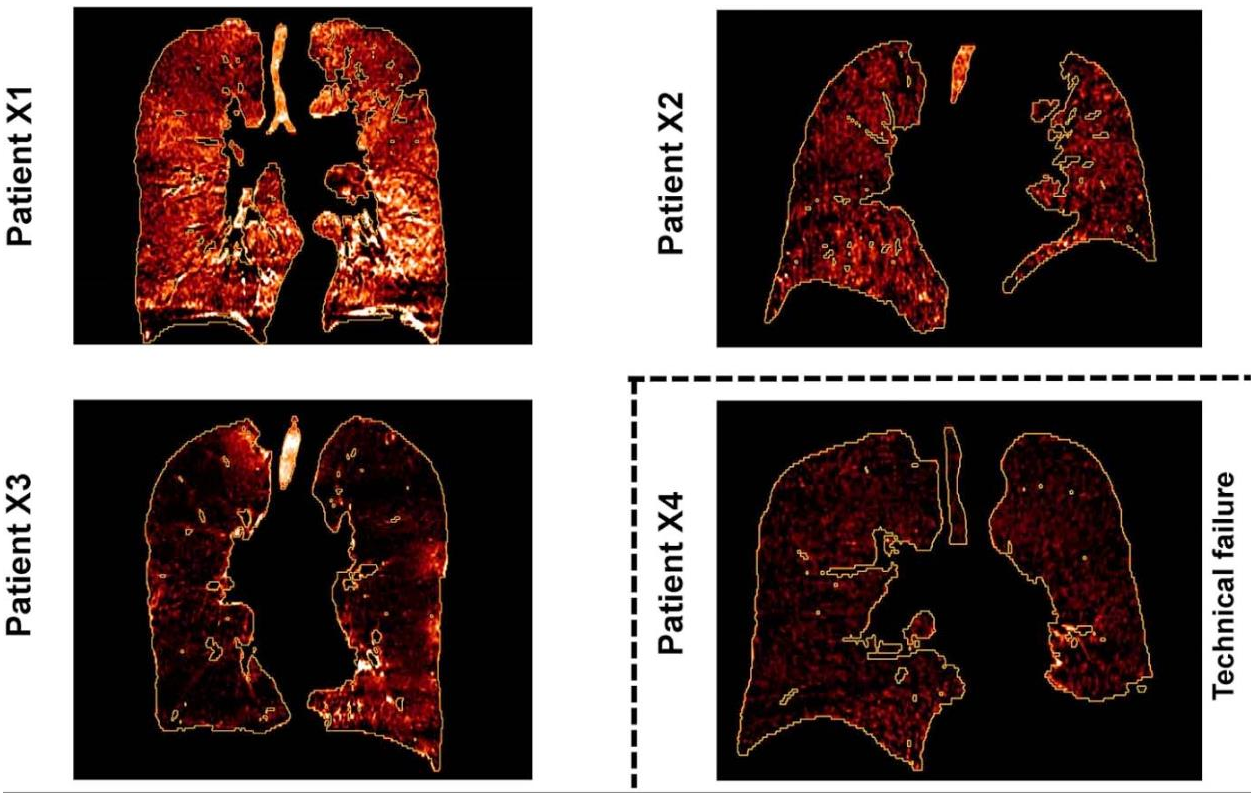

Figure A2. Xenon-enhanced computed tomography image for four patients who did not receive the concurrent (but optional) ventilation single-photon emission computed tomography-computed tomography image during the study. Another advantage for xenon-enhanced computed tomography-based ventilation is that single-photon emission computed tomography hardware is not often accessible to patients undergoing radiation therapy.